Catalysis Today 158 (2010) 329–335

Contents lists available at ScienceDirect

Catalysis Today

journal homepage: www.elsevier.com/locate/cattod

TiO_2/SBA-15 photocatalysts synthesized through the surface acidolysis of $Ti(O^nBu)_4$ on carboxyl-modified SBA-15

Shucui Zhang[a,c], Dong Jiang[a,*], Tao Tang[a,c], Junhua Li[a,c], Yao Xu[a,*], Wanling Shen[b,c], Jun Xu[b], Feng Deng[b]

[a] State Key Laboratory of Coal Conversion, Institute of Coal Chemistry, Chinese Academy of Sciences, 27 Taoyuan Nan Road, Taiyuan 030001, Shanxi, China
[b] State Key Laboratory of Magnetic Resonance and Atomic and Molecular Physics, Wuhan Institute of Physics and Mathematics, Chinese Academy of Sciences, Wuhan 430071, China
[c] Graduate University of the Chinese Academy of Sciences, Beijing 100049, China

ARTICLE INFO

Article history:
Available online 18 May 2010

Keywords:
TiO_2
Mesoporous materials
Acidolysis
Photocatalysis

ABSTRACT

Based on an acidolysis reaction between titanium *n*-butoxide and carboxyl (COOH) groups, serial highly dispersed TiO_2 photocatalysts were successfully synthesized on COOH-modified mesoporous SBA-15 material. Even after calcined at 550 °C to improve the crystallization, the TiO_2/SBA-15 products possessed high surface area above 400 $m^2\ g^{-1}$ that should be attributed to the high porosity of mesoporous SBA-15 and the highly uniform COOH group distribution in mesopores. HRTEM images revealed that TiO_2 nanocrystals dispersed well on the surface of SBA-15. The pore channels were partly blocked by TiO_2 nanocrystals, resulting in a bimodal pore size distribution in TiO_2/SBA-15 compared with SBA-15. XRD and Raman results disclosed the exclusive anatase phase of TiO_2 in the photocatalysts. With adjusting the molar ratio of COOH to TB, the TiO_2/SBA-15 products displayed different photocatalytic performance using Rhodamine B as probe under UV light.

1. Introduction

Heterogeneous semiconductor photocatalysts, such as TiO_2, ZnO, ZnS and SnO_2, have attracted extensive attention because of their applications in environment protection [1,2]. Compared with other semiconductors, TiO_2 exhibits remarkable advantages including low-cost, high photocatalytic efficiency, chemical stability and environmental friendliness, and has become a very promising photocatalyst [3,4]. Generally, the produced TiO_2 has relatively low surface area that results in a low adsorption ability and further poor photocatalytic activity. Therefore, it can be concluded that increasing surface area of TiO_2 may be an effective way to improve its photocatalytic activity [5]. Recently, many efforts have been made on supporting TiO_2 on porous adsorbents such as zeolite, mesoporous silica and activated carbon [6]. As an ideal catalytic support, mesoporous silica has attracted great attention due to its high surface area, adjustable pore size, ordered frameworks, and transparent to UV radiation [7]. Among the various mesoporous silica supports, SBA-15 is currently considered as one of the most prominent mesoporous silica supports due to its desirable features of high surface area, uniform large pore size distribution and long-term stability [8–10]. Such mesoporous SBA-15 supported TiO_2 material takes the advantages of both TiO_2 and SBA-15.

To prepare TiO_2/SBA-15 photocatalyst, direct synthesis and post-synthesis are two generally used methods. The procedure of direct synthesis of TiO_2/SBA-15 photocatalyst is to incorporate TiO_2 and SiO_2 precursors into synthetic solution and subsequently introduce TiO_2 species into mesoporous SBA-15 structure [11–14]. The approach of post-synthesis is to deposit TiO_2 on the surface of the pre-prepared mesoporous SBA-15 material via applying the methods of solvent evaporation impregnation [15,16], precipitation [17], or grafting [18,19]. However, such methods have some obvious shortcomings. For direct synthesis, although Ti species have a good distribution on SBA-15 framework, the obtained TiO_2/SBA-15 photocatalyst normally possesses low surface area [20] and the loading amount of TiO_2 greatly affects the formation of mesoporous structure [21]. For the later method, it is little difficult to control the loading amount of TiO_2 and the as-obtained TiO_2/SBA-15 photocatalyst has no good dispersibility of TiO_2 on the surface of SBA-15 [22]. Therefore, it is necessary to explore a new synthetic strategy to avoid the shortcomings revealed in above-mentioned methods.

Based on our previous work, well-crystallized TiO_2 nanoparticles were synthesized under solvothermal condition using acetic acid (AcOH) and titanium *n*-butoxide (TB) as reactants [23] and

* Corresponding authors. Tel.: +86 351 4049859; fax: +86 351 4041153.
E-mail addresses: jdred@sxicc.ac.cn (D. Jiang), xuyao@sxicc.ac.cn (Y. Xu).

0920-5861/$ – see front matter © 2010 Elsevier B.V. All rights reserved.
doi:10.1016/j.cattod.2010.04.004

carboxyl-modified SBA-15 (COOH/SBA-15) with high content and high dispersibility of COOH groups was synthesized [24]. Here, combining these two concepts, we will report a novel route to synthesize TiO_2/SBA-15 photocatalysts with high photocatalytic activity through acidolysis reaction between surface COOH groups of COOH/SBA-15 and TB. The good dispersed COOH groups on the surface of COOH/SBA-15 could coordinate with the TB molecules to anchor them. After solvothermal treatment, TB molecules were transformed into TiO_2 nanoparticles and finally formed TiO_2/SBA-15 photocatalysts and calcination of the as-synthesized TiO_2/SBA-15 was used to improve the crystallization of TiO_2 and remove the organic compounds. With serial TiO_2/SBA-15 products, high photocatalytic performance has been obtained using Rhodamine B (RhB) as probe under UV light.

2. Experimental

2.1. Synthesis of photocatalysts

In the present study, all chemical reagents were used without further purification. COOH/SBA-15 was synthesized according to our previous work [24] using triblock polymer Pluronic P123 as template and tetraethoxysilane (TEOS), (2-cyanoethyl) triethoxysilane (CETES) as the silica sources under acidic condition. In a typical synthesis of COOH/SBA-15, 4.0 g P123 and 4.0 g KCl were dissolved in 120.0 ml of 2.0 M HCl solution at 40 °C. After the mixture was stirred vigorously for about 5 h, CETES (5.0 ml) was added to the above solution and hydrolyzed for up to 0.5 h under stirring. TEOS (5.0 ml) was then added into the mixture slowly. Next, the resultant mixture was stirred for 24 h at 40 °C, followed by aging for 36 h at 90 °C under static condition. The product cyanide-modified (CN/SBA-15) was filtered, washed with water and absolute ethanol, and then dried at 60 °C. Afterwards, 1.0 g of CN/SBA-15 was treated with 150.0 ml of H_2SO_4 (48 wt.%) solution for 24 h at 95 °C to cleave the template and to oxidize the CN groups to COOH groups. The final solid product was washed with water repeatedly and then dried at 60 °C.

TiO_2/SBA-15 photocatalysts were synthesized using titanium *n*-butoxide (TB) and COOH/SBA-15 as reactants. Typically, 1.0 g COOH/SBA-15 powder was dispersed in a solution containing 0.5 ml TB and 20.0 ml acetic ether. The mixture was stirred for 30 min at room temperature. The resultant solution was then transferred into a Teflon-lined stainless autoclave and solvothermally treated at 220 °C for 12 h. After naturally cooling to room temperature, the resultant product was washed three times with absolute ethanol and dried at 60 °C for 12 h and finally the solids were calcined in air at 550 °C for 4 h at a heating rate of 1 °C/min. The obtained TiO_2/SBA-15 sample was designated as TSAc*x*, where *x* represented the molar ratio of COOH to TB.

For comparison, PTS photocatalyst (TiO_2 supported on SBA-15 unmodified with COOH groups) was synthesized following the impregnation method [22] using SBA-15 and TB as starting materials, in which the TiO_2 loading amount was same as that of TSAc5. In addition, pure TiO_2 was also synthesized according to the literature [23].

2.2. Characterization of samples

The X-ray diffraction (XRD, Cu Kα, 40 kV, 40 mA, D8, Advance Bruker Axs) was used for studying the phase composition. The experiments for ^{29}Si MAS NMR (MSL-400, Bruker) were performed at a resonance frequency of 79.5 Hz. Raman spectra (HR-800, Jobin–Yvon Labram) were recorded. Chemical structure information of samples was collected using FT-IR spectra (Nicolet-470) with 4 cm^{-1} resolution. The surface element composition and the bonding situation of the samples were determined by X-ray photoelectron spectroscopy (XPS, Mg Kα, PHI-5300X, PerkinElmer Physics Electronics). The BET surface area was measured with nitrogen adsorption at 77 K (Tristar-3000, Micromeritics). The morphology and mesoporous structure of samples were observed on a high-resolution transmission electron microscopy (JEOL-2010).

2.3. Photodegradation of Rhodamine B (RhB)

The photocatalytic performance of TiO_2/SBA-15 photocatalyst was studied by measuring the degradation of RhB in aqueous solution under UV light irradiation. A 300-W Hg lamp ($\lambda = 365$ nm) was used as the light source and positioned inside a cylindrical Pyrex vessel surrounded by a circulating water jacket to cool the lamp. Aqueous photocatalyst dispersion was prepared by adding 500 mg photocatalyst to a 500 ml solution containing RhB at an appropriate concentration of 50 ppm (C_0). In all experiments, prior to irradiation, the suspension of photocatalyst in RhB solution was stirred in the dark for 40 min to achieve an RhB adsorption/desorption equilibrium. The concentration of RhB at this point was considered as the absorption equilibrium concentration C_e. The adsorption capacity of photocatalyst to RhB was defined by the adsorption amount of RhB on photocatalyst, which was equal to $(C_0 - C_e)$. At given irradiation time intervals, the dispersion was sampled (5 ml). The supernates (C_t) were analyzed using a TU-1901 UV–vis spectrometer to determine the concentration of RhB. The degradation percentage of RhB after 40 min UV light irradiation was calculated by the formula: degradation percentage = $(1 - C_t/C_0) \times 100\%$. And the photocatalytic decomposition of RhB molecules followed the Langmuir–Hinshelwood kinetic model. The first-order linear relationship was revealed by the plots of the $\ln(C_0/C_t)$ versus irradiation time (t), where C_t was the concentration of RhB, C_0 was the initial concentration of RhB, and t was the irradiation time.

3. Results and discussion

3.1. Formation of TiO_2/SBA-15 photocatalysts

The synthetic process of TiO_2/SBA-15 photocatalyst is schematically presented in Scheme 1. The whole synthesis of TiO_2/SBA-15 photocatalyst is divided into three steps: (1) synthesis of COOH/SBA-15. CN/SBA-15 was synthesized at first by the P123-templated co-condensation of the silica source TEOS and the functional silane CETES, in which the molecular-level assembly process made CN groups disperse evenly on the surface of SBA-15. Then after further oxidizing the CN groups with sulfuric acid, highly dispersed COOH groups would be obtained on the pore sur-

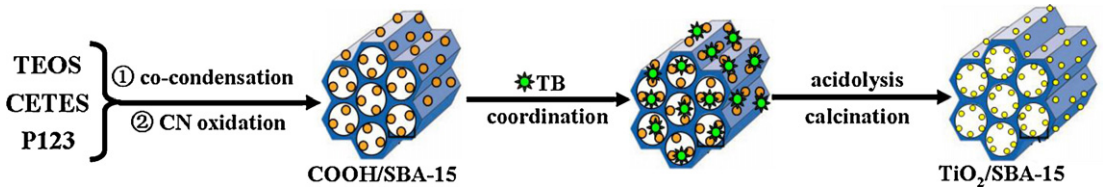

Scheme 1. Flow chart of TiO_2/SBA-15 synthesis.

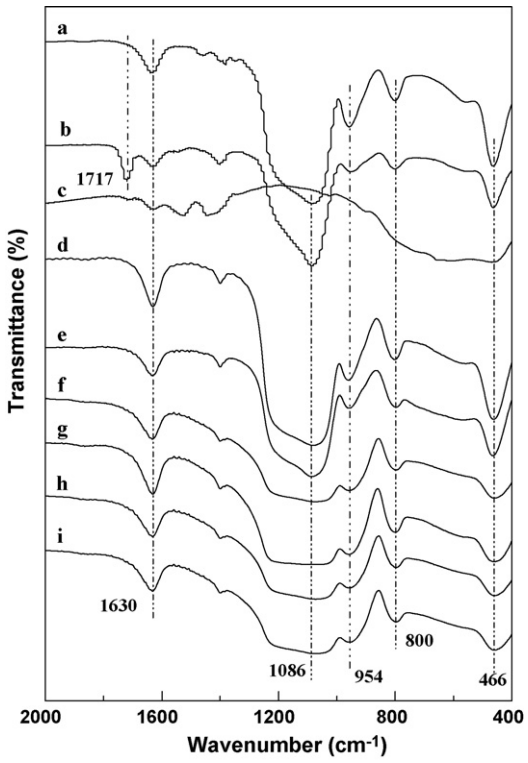

Fig. 1. FT-IR spectra of samples (a) SBA-15, (b) COOH/SBA-15, (c) TiO_2, (d) TSAc2, (e) TSAc3, (f) TSAc4, (g) TSAc5, (h) TSAc6, and (i) TSAc7.

face of SBA-15. (2) The acidolysis reaction of surface COOH groups and the synthesis of TiO_2/SBA-15. Firstly, the good dispersed COOH groups on the surface of COOH/SBA-15 may serve as anchor sites to coordinate with the TB molecules to produce acetate ligands: $(Si(OEt)_3–C_2H_5–CO_2)_xTi(n BuO)_{4-x}$. Subsequently, the ligands were to generate TiO_2 nanoparticles by solvothermal treatment and formed TiO_2/SBA-15 products. (3) Calcination of the as-synthesized TiO_2/SBA-15 to improve the crystallization of TiO_2 and remove the organic compounds.

FT-IR spectra of SBA-15, COOH/SBA-15, TiO_2 and TiO_2/SBA-15 photocatalysts are shown in Fig. 1. The absorption band appearing at about 1630 cm^{-1} can be attributed to the water adsorbed on the samples surface. Compared with SBA-15 in the spectra, a strong adsorption band was observed at about 1717 cm^{-1} for COOH/SBA-15 sample, which should be attributed to the characteristic vibration of COOH [23]. The appearance of the peak at 1717 cm^{-1} indicates the successful introduction of COOH groups to SBA-15 mesopores. Moreover, in order to accurately measure the content of COOH groups on COOH/SBA-15 sample, ^{29}Si MAS NMR spectra are applied to provide the local bonding information around Si atom and the content of COOH. The ^{29}Si MAS NMR spectrum of COOH/SBA-15 is presented in Fig. 2. Three resonances at −110, −101, and −92 ppm can be assigned to Q^4, Q^3 and Q^2 species in the silica framework [$Q^n = Si(OSi)_n(OH)_{4-n}$, $n = 2-4$], respectively. The two resonances at −65 and −55 ppm are attributed to T^3 and T^2 [$T^m = COOH–Si(OSi)_m(OH)_{3-m}$, $m = 1–3$]. From Fig. 2, compared with SBA-15, the signals assigned to T-band of COOH/SBA-15 appear, suggesting the existence of COOH groups. The corresponding integral intensity of each resonance signal from ^{29}Si MAS NMR spectra are collected in Table 1. It is found that the content of COOH groups in COOH/SBA-15 can be up to 61.4%.

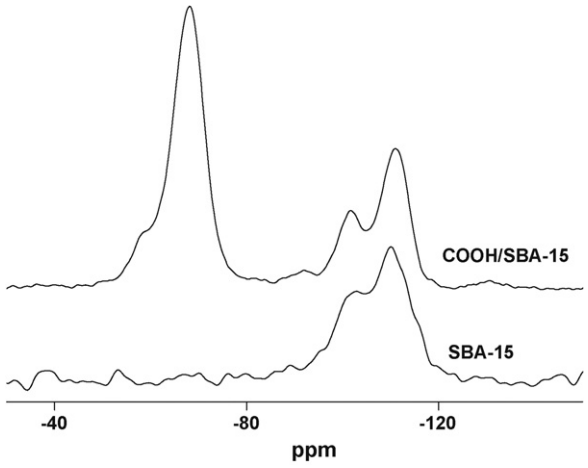

Fig. 2. ^{29}Si MAS NMR spectra of samples SBA-15 and COOH/SBA-15.

Table 1
^{29}Si MAS NMR data of SBA-15 and COOH/SBA-15.

Sample	Relative integral intensity (%)					COOH content (%)[a]
	Q^4	Q^3	Q^2	T^3	T^2	
SBA-15	63.2	32.3	4.5	–	–	–
COOH/SBA-15	23.1	12.9	2.6	51.7	9.7	61.4

[a] Calculated using equation: $(T^3 + T^2)/(Q^4 + Q^3 + Q^2 + T^3 + T^2)$.

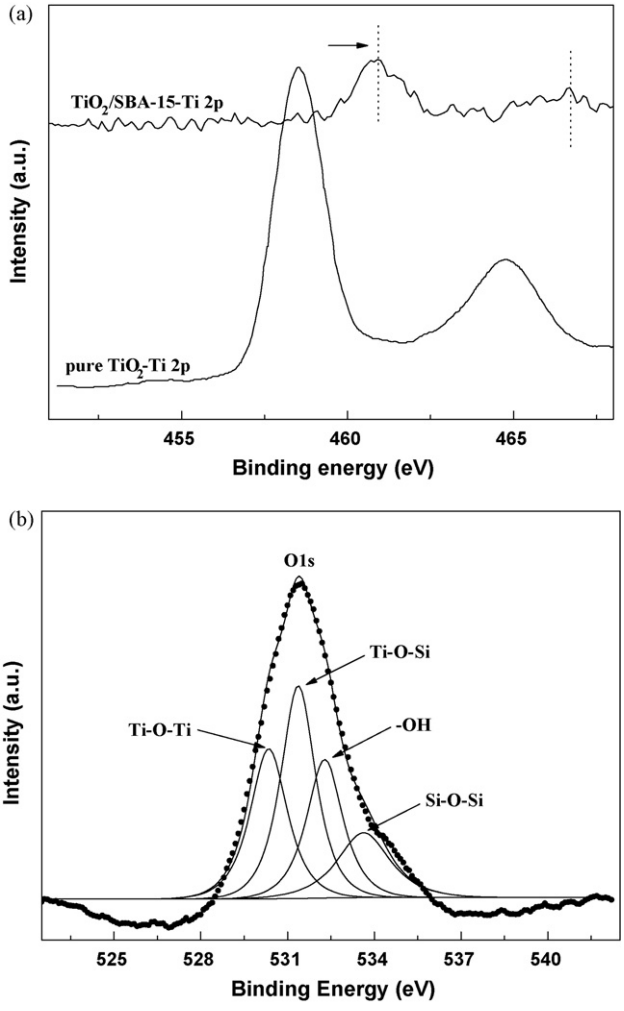

Fig. 3. High-resolution XPS spectra of TSAc5 sample: (a) Ti 2p region and (b) O 1s region.

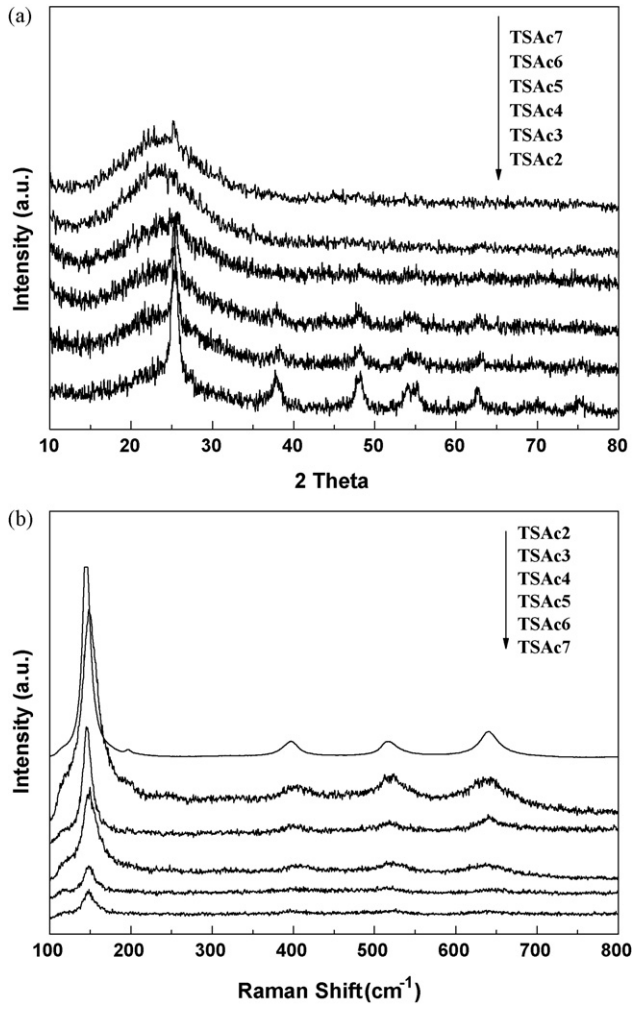

Fig. 4. (a) XRD patterns and (b) Raman spectra of TiO_2/SBA-15 photocatalysts.

Compared with TiO_2, the absorption bands around 1086, 800 and 466 cm^{-1} can be observed in all the TiO_2/SBA-15 photocatalysts (see Fig. 1), which can be assigned to the asymmetric stretching, symmetric stretching and deformation modes of Si–O–Si [25], respectively. Additionally, as shown in the spectra of all the samples except TiO_2, a band at about 954 cm^{-1} is clearly observed. Theoretically, IR bands observed at 910–960 cm^{-1} may be assigned to the stretching vibration of Ti–O–Si [26,27], and the symmetric stretching vibration of Si–OH groups is also in the 940–960 cm^{-1} [28]. Thus, this peak at 954 cm^{-1} indicates the existence of Ti–O–Si bond and/or associates with non-condensed Si–OH groups.

To further prove the structure of TiO_2/SBA-15 photocatalysts, XPS as a surface characterization technique is also used to investigate the surface element bonding structure of TiO_2/SBA-15 samples. The high-resolution XPS spectra of TSAc5 sample are exhibited in Fig. 3. In the Ti 2p region (see Fig. 3a), an obvious shift to higher binding energies is observed relative to TiO_2. The result can be due to the chemical interaction between TiO_2 and SBA-15, suggesting the formation of Ti–O–Si [29]. From Fig. 3b, the profile of TSAc5 sample can be fit by three Lorentzian curves appearing at 533.6, 531.4 and 530.3 eV, which can be attributed to Si–O–Si, Ti–O–Si and Ti–O–Ti components [30], respectively, while the peak at around 532.3 eV can be assigned to surface hydroxyl [31]. The result also shows that a new bond Ti–O–Si has formed in TSAc5 sample, and is in good agreement with the FT-IR spectra result. It is well known that the presence of Ti–O–Si chemical bond

Table 2
The BET surface areas and the Ti density of TiO_2/SBA-15 samples.

Samples	COOH/TB molar ratio	S_{BET} ($m^2\ g^{-1}$)	Ti density (nm^{-2})
TSAc2	2	408.6	5.4
TSAc3	3	420.6	3.5
TSAc4	4	426.5	2.6
TSAc5	5	446.2	2.0
TSAc6	6	444.3	1.6
TSAc7	7	440.2	1.4

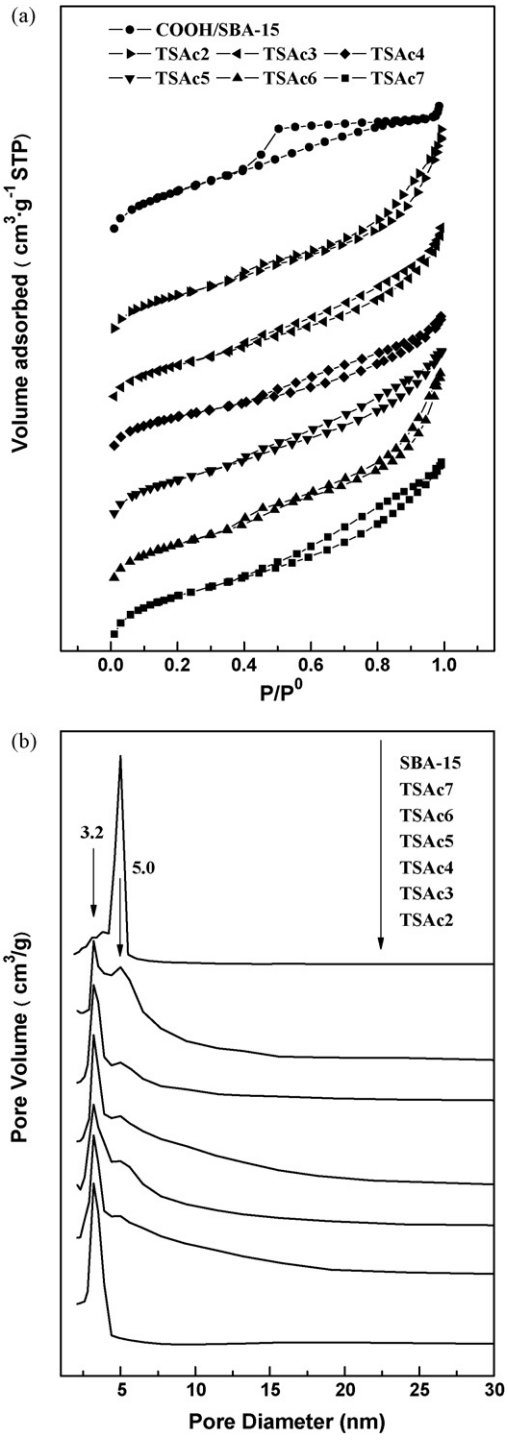

Fig. 5. (a) N_2 sorption isotherms and (b) pore size distributions of SBA-15 and TiO_2/SBA-15 samples.

can enhance the surface acidity of TiO_2/SBA-15 [32] and form the surface defects [33], which would benefit to improve the photocatalytic activity of TiO_2/SBA-15 photocatalysts.

From the XRD patterns of all TiO_2/SBA-15 photocatalysts (as shown in Fig. 4a), the samples TSAc2, TSAc3, and TSAc4 with lower COOH/TB molar ratio (high TiO_2 content) have five distinctive peaks at 2θ of 25.3°, 37.8°, 48.1°, 53.9°, 55.2°, corresponding to the (1 0 1), (0 0 4), (2 0 0), (1 0 5) and (2 1 1) crystal planes of anatase, respectively, according to JCPDS File No. 21–1272. Only a faint (1 0 1) reflection can be identified for the other TiO_2/SBA-15 samples with COOH/TB molar ratio above 4. The other invisible diffraction peaks attributed to anatase TiO_2 may display that the characteristic peaks of TiO_2 are overlapped by the diffraction peak of SBA-15, owing to the low TiO_2 content. It can be seen that the intensity of the (1 0 1) diffraction peak becomes strong with the decrease of COOH/TB molar ratio, that is, with the increase of TiO_2 content. The XRD result can be further confirmed by the Raman spectroscopy (Fig. 4b). Raman spectra of all TiO_2/SBA-15 samples reveal four Raman bands at 146, 399, 517 and 640 cm^{-1} ranging between 100 and 800 cm^{-1}. All the Raman peaks can be assigned to the E_g, B_{1g}, A_{1g} and E_g modes of the anatase phased TiO_2 [34,35]. No any Raman peaks of impurity can be observed. The XRD and Raman results clearly indicate that anatase is the exclusive titania phase present in these samples, suggesting the high purity of the samples.

3.2. Pore structure and morphography

In order to understand the effect of TiO_2 existence on the mesoporous structure, the nitrogen sorption isotherms at 77 K are shown in Fig. 5a. According to the IUPAC convention, the isotherms of COOH/SBA-15 can be classified as type IV that is typical of mesoporous materials [36], showing that COOH modification has no effect on the mesoporous structure of SBA-15. However, there is an obvious difference in the shape of the hysteresis loops between COOH/SBA-15 and the TiO_2/SBA-15 photocatalysts. With the formation of TiO_2 species, the hysteresis loop changes to the H3-type corresponding to the confined gap pore, resulted from the filling of SBA-15 pores by TiO_2 nanocrystals. Moreover, the BET surface areas of the TiO_2/SBA-15 photocatalysts are listed in Table 1.

The pore size distribution calculated from the desorption branches using the BJH method is shown in Fig. 5b. It is found that SBA-15 shows a narrow pore size distribution with the diameter of 5.0 nm. Compared with SBA-15, all photocatalysts display a new distribution at around 3.2 nm. More interestingly, the distribution at 3.2 nm becomes stronger and stronger with the increase of TiO_2 content (decrease of COOH/TB molar ratio) while the distribution at 5.0 nm gradually disappears. With the largest TiO_2 content, the distribution of TSAc2 at 5.0 nm completely disappears, only single-modal pore size distribution at 3.2 nm can be found. The trend in the pore size distribution indicates that TiO_2 nanoparticles are formed evenly on the surface of SBA-15. Furthermore, the Ti density (the number of Ti atoms on unit pore surface) is calculated by dividing the total number of Ti atoms on per gram of SBA-15 with its BET surface area. Obviously, the Ti density gradually increases with the increase of TiO_2 content (see Table 2). The Ti density 5.4 nm^{-2} is very close to the theoretical value 5.5 nm^{-2} of the Ti density on the anatase (0 1 0) plane [37], showing that the mesopore surface has been covered by a nearly complete TiO_2 monolayer [38]. From sample TSAc7 to TSAc2, the trends in the pore distribution and the Ti density reveal the covering extent of TiO_2 nanoparticles on mesopore surface. This obvious trend in mesoporous structure should be correlated with the accurate acidolysis reaction between highly

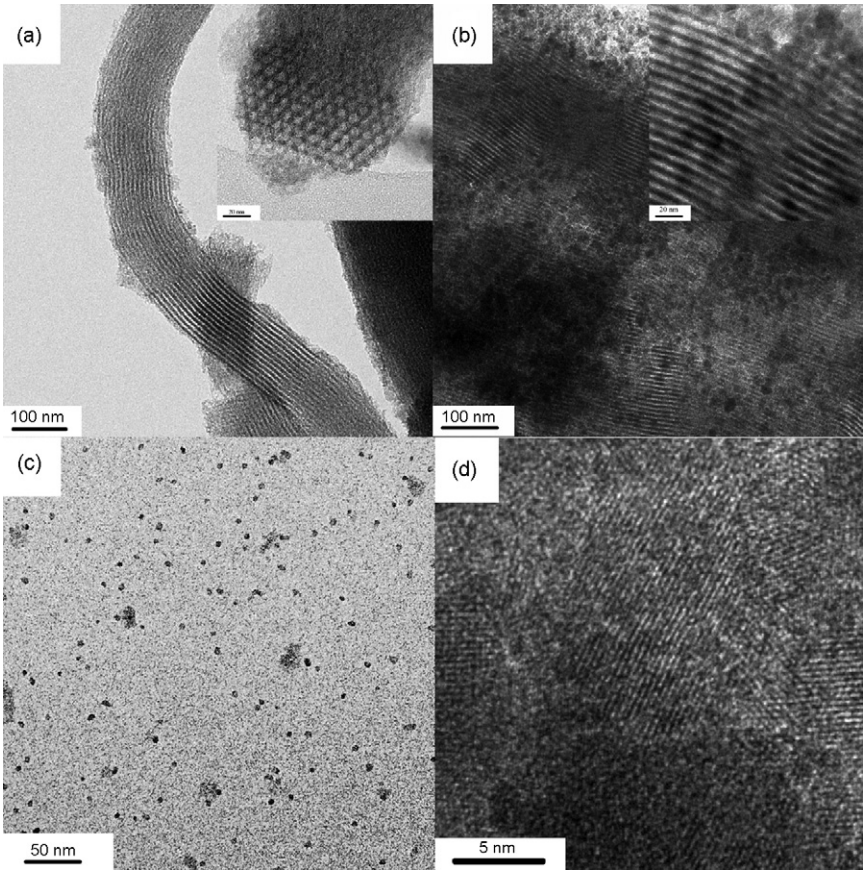

Fig. 6. HRTEM images of (a) COOH/SBA-15 and (b–d) TSAc7 sample.

dispersed COOH groups and TB molecules. Therefore, it is reasonable to conclude that the synthetic process is efficient to disperse TiO_2 nanocrystals on the surface of SBA-15.

Direct evidences from HRTEM images can be used to confirm the formation of TiO_2 nanocrystals on the mesopores and the effect of TiO_2 on the pore structure of TiO_2/SBA-15 photocatalyst. Fig. 6 shows the HRTEM images of the samples COOH/SBA-15 and TSAc7. From Fig. 6a, COOH/SBA-15 shows the regular hexagonal array of mesopores with one-dimensional channel indicating a 2D hexagonal mesostructure. As shown in Fig. 6b, the introduction of TiO_2 does not destroy the ordered array of mesopores and TiO_2 nanocrystals disperse well on the surface of SBA-15. With higher magnification of TEM image (the inset of Fig. 6b), it can be clearly seen that the mesopore channels have been occupied partly. In detail, the more white channels mean less occupation. Therefore the bimodal pore size distribution should be understandable. To further display the dispersibility of TiO_2 nanoparticles, the sample TSAc7 was etched by a HF (hydrofluoric acid) solution to remove the silica framework and obtain the TiO_2 nanoparticles. The TEM image of the as-obtained TiO_2 nanoparticles (see Fig. 6c) clearly shows the high dispersibility of TiO_2 nanoparticles with about 4 nm size in diameter. From Fig. 6d, the lattice fringe of TiO_2 can be clearly observed with the average *d*-spacing of about 0.352 nm, corresponding to the (1 0 1) reflection of the anatase phase.

3.3. Photocatalytic performance of TiO_2/SBA-15

Before testing the photocatalytic performance, the RhB adsorption capacity of photocatalyst (as shown in Fig. 7a) must be investigated at first because it is very important for the performance. The RhB adsorption capacities of TiO_2/SBA-15 photocatalysts are evaluated by the adsorption amount ($C_0 - C_e$) of RhB. The higher value of adsorption amount means the stronger adsorption of RhB on photocatalysts. It is noticeable that the adsorption capacity of TiO_2/SBA-15 samples increases with the increase of COOH/TB molar ratio, reaches the highest value at COOH/TB molar ratio = 5, and then decreases. It is well known that the adsorption capacity is mainly determined by surface area and surface chemical property of photocatalyst [39]. Therefore, it is undoubted that larger surface area of TSAc5 sample (446.2 $m^2\,g^{-1}$) benefits the adsorption of RhB. From sample TSAc2 to TSAc7, the TiO_2 content gradually decreases but the surface area increases a little. The small difference in surface area cannot affect largely the adsorption of RhB. The slight decrease of adsorption capacity of TSAc6 and TSAc7 should result from the decrease of the TiO_2 content.

To clearly compare the photocatalytic performances of various photocatalysts, the degradation kinetic curves within 40 min UV light irradiation are shown in Fig. 7b. It is found that all TSAc photocatalysts are higher than those of pure TiO_2 and PTS. In general, the photocatalytic activity depends on the crystallinity, the dispersion of TiO_2 [40], and the adsorption capacity to reactant [41,42]. Compared to the TSAc photocatalysts, the pure TiO_2 exhibits lower photocatalytic activity, which should be attributed to the lower adsorption capacity decided by its small surface area of 139.6 $m^2\,g^{-1}$ (see Fig. 7a). PTS sample possesses very high adsorption capacity because of its large surface area of 612.5 $m^2\,g^{-1}$ (see Fig. 7a), unfortunately, its poor dispersibility of TiO_2 finally resulted in a quite low photocatalytic activity. Combining with the above analyses, it can be concluded that the good dispersibility of TiO_2 nanocrystals and the high adsorption capacity benefit the photoactivity of TSAc photocatalysts.

The photodegradation percentage in different COOH/TB molar ratio is also shown in Fig. 7a. For the TSAc photocatalysts, with the increase of COOH/TB molar ratio from 2 to 7, the photocatalytic activity increases, reaches the highest value at the COOH/TB molar ratio = 5, and then decrease. On the whole, the change trend of photocatalytic performance is in agreement with that of adsorption capacity. Nevertheless, it is noticeable that the adsorption capacity from TSAc5 to TSAc7 exhibits a slow decline, and a rapid decrease is found in the photocatalytic performance. In our experiments, all TSAc photocatalysts possess good dispersion of TiO_2, therefore the differences should be attributed to the combination effect of the adsorption capacity and the crystallinity. From sample TSAc2 to TSAc7, the adsorption capacity (positive factor) is enhanced with the increase of the surface area and the pore size, but the crystallinity decreases gradually due to the reduced loading amounts of TiO_2 (negative factor). Finally, the photocatalytic performances of TSAc photocatalysts reach the highest value at COOH/TB molar ratio = 5.

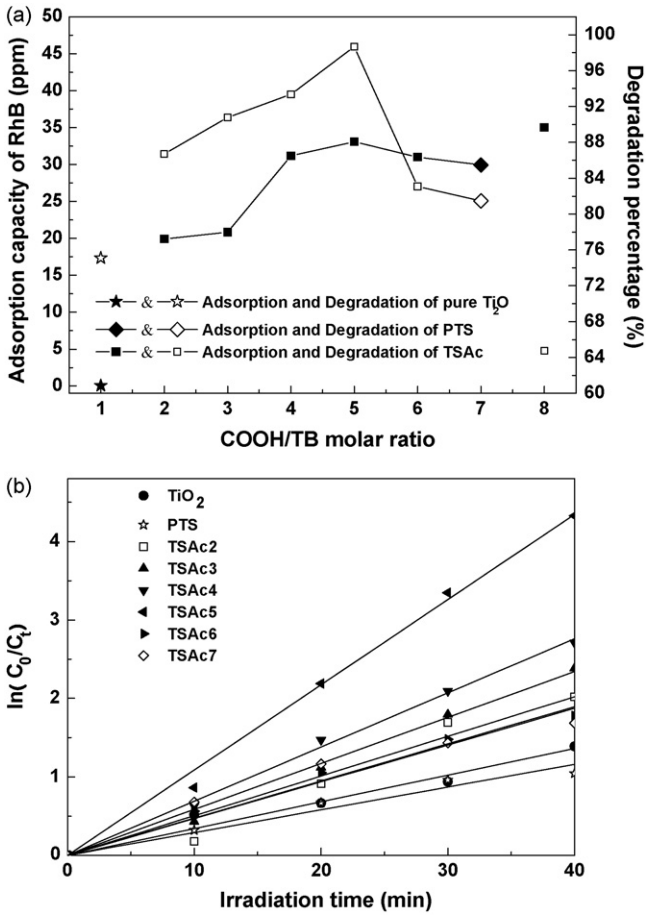

Fig. 7. (a) Adsorption capacity (AC) and degradation percentage (DP), (b) degradation kinetics within 40 min UV light irradiation of TSAc photocatalysts, PTS and pure TiO_2.

4. Conclusions

In summary, serial highly dispersed TiO_2/SBA-15 photocatalysts were successfully synthesized based on an acidolysis reaction between titanium *n*-butoxide (TB) and well-dispersed carboxyl (COOH) groups on carboxyl-modified SBA-15. As-prepared TiO_2/SBA-15 photocatalysts exhibited an improved UV photocatalytic performance of decompositing RhB because of the high adsorption capacity of photocatalysts and the good dispersion of TiO_2 on the surface of SBA-15. Moreover, the synthetic method may be extended further to the preparation of photocatalyst for the visible photocatalytic applications.

Acknowledgment

The financial support from SKLCC in-house project (No. 2008BWZ011) was acknowledged.

References

[1] Z.S. Wang, F.Y. Li, N.Q. Li, J. Phys. Chem. B 104 (2000) 9676.
[2] J. Aguado, R. van Grieken, M.J. López-Muñoz, J. Marugán, Catal. Today 75 (2002) 95.
[3] K.L. Frindell, M.H. Bartl, A. Popitsch, G.D. Stucky, Angew. Chem. Int. Ed. 41 (2002) 959.
[4] Z.B. Zhang, C.C. Wang, R. Zakaria, J.Y. Ying, J. Phys. Chem. B 102 (1998) 10871.
[5] B.I. Lemon, J.T. Hupp, J. Phys. Chem. B 103 (1999) 3797.
[6] D. Morris, R.G. Egdell, J. Mater. Chem. 11 (2001) 3207.
[7] T. Gao, G. Meng, Y. Tian, S. Sun, X. Liu, L. Zhang, J. Phys.: Condens. Matter 14 (2002) 12651.
[8] D. Zhao, J. Feng, Q. Huo, N. Melosh, G.H. Fredrickson, B.F. Chmelka, G.D. Stucky, Science 279 (1998) 548.
[9] D. Zhao, Q. Huo, J. Feng, B.F. Chmelka, G.D. Stucky, J. Am. Chem. Soc. 120 (1998) 6024.
[10] P. Cheng, M.P. Zheng, Y.P. Jin, Q. Huang, M.Y. Gu, Mater. Lett. 57 (2003) 2989.
[11] Y. Chen, Y. Huang, J. Xiu, X. Han, X. Bao, Appl. Catal. A: Gen. 273 (2004) 185.
[12] P.V. Messina, P.C. Schulz, J. Colloids Interface Sci. 299 (2006) 305.
[13] T. Hoshikawa, T. Ikebe, M. Yamada, R. Kikuchi, K. Eguchi, J. Photochem. Photobiol. A: Chem. 184 (2006) 78.
[14] J. Jime′nez-Jime′nez, M. Rubio-Alonso, A. Jime′ne-Lopez, J. Phys. Chem. Solids 67 (2006) 1007.
[15] Y.H. Hsien, C.F. Chang, Y.H. Chen, S. Cheng, Appl. Catal. B 31 (2001) 241.
[16] A.A. Belhekar, S.V. Awate, R. Anand, Catal. Commun. 3 (2002) 453.
[17] A. Hanprasopwattana, S. Srinivasan, A.G. Sault, A.K. Datye, Langmuir 12 (1996) 3173.
[18] W. Yan, B. Chen, S.M. Mahurin, E.W. Hagaman, S. Dai, S.H. Overbury, J. Phys. Chem. B 108 (2004) 2793.
[19] M. Widenmeyer, S. Grasser, K. K¨ohler, R. Anwander, Micropor. Mesopor. Mater. 327 (2001) 44.
[20] K.D. Witte, A.M. Busuioc, V. Meynen, Micropor. Mesopor. Mater. 110 (2008) 100.
[21] W.Y. Dong, Y.J. Sun, C.W. Lee, J. Am. Chem. Soc. 129 (2007) 13894.
[22] R. van Grieken, J. Aguado, M.J. López-Muñoz, J. Marugán, Photochem. Photobiol. A: Chem. 148 (2002) 315.
[23] D. Jiang, Y. Xu, D. Wu, Y.H. Sun, Eur. J. Inorg. Chem. (2008) 1236.
[24] W.J. Xu, Q. Gao, Y. Xu, J. Solid State Chem. 181 (2008) 2837.
[25] K.Y. Jung, S.B. Park, Appl. Catal. B 25 (2000) 249.
[26] S. Kein, S. Thorimbert, W.F. Maier, J. Catal. 163 (1996) 476.
[27] D.W. Lee, S.K. Ihm, K.H. Lee, Chem. Mater. 17 (2005) 4461.
[28] M. Llusar, G. Monros, C. Roux, J.L. Pozzo, C. Sanchez, J. Mater. Chem. 13 (2003) 2505.
[29] M. Ramirez-Del-Solar, N. de la Rosa-Fox, L. Esquivas, J. Zarzycki, J. Non-Cryst. Solids 121 (1990) 84.
[30] Z.L. Hua, J.L. Shi, L.X. Zhang, M.L. Ruan, J.N. Yan, Adv. Mater. 14 (2002) 830.
[31] C. Xie, Z. Xu, Q.J. Yang, B.Y. Xue, Y.G. Du, J.H. Zhang, Mater. Sci. Eng. B 112 (2004) 34.
[32] J.Y. Zhang, Q. Li, W.L. Cao, J. Inorg. Chem. 20 (2004) 725.
[33] Z.J. Li, B. Hou, Y. Xu, J. Colloids Interface Sci. 288 (2005) 149.
[34] T. Ohsaka, F. Izumi, Y.J. Fujiki, Raman Spectrosc. 7 (1978) 321.
[35] T.J. Ohsaka, Phys. Soc. Jpn. 48 (1980) 1661.
[36] K.S.W. Sing, D.H. Everett, J. Rouquol, Pure Appl. Chem. 57 (1985) 603.
[37] X. Gao, S.R. Bare, J.L.G. Fierro, M.A. Banares, I.E. Wachs, J. Phys. Chem. B 102 (1998) 5653.
[38] Z.H. Luan, M.M. Estelle, P.A.W. van der Heide, D.Y. Zhao, R.S. Czemuszewicz, L. Kevan, Chem. Mater. 11 (1999) 3680.
[39] D. Jiang, Y. Xu, D. Wu, Y.H. Sun, J. Solid State Chem. 181 (2008) 593.
[40] L. Zhao, J.G. Yu, J. Colloids Interface Sci. 304 (2006) 84.
[41] C. Minero, F. Catozzo, E. Pelizzetti, Langmuir 8 (1992) 481.
[42] C. Kormann, D.W. Bahnemann, M.R. Hoffmann, Environ. Sci. Technol. 25 (1991) 494.